IEEE Access
Multidisciplinary | Rapid Review | Open Access Journal

IEEE ENGINEERING IN MEDICINE AND BIOLOGY SOCIETY SECTION

Received 5 February 2024, accepted 10 April 2024, date of publication 15 April 2024, date of current version 29 April 2024.

Digital Object Identifier 10.1109/ACCESS.2024.3389492

THEORY

Biomechanical Effects of Anterior Decompression and Fusion With Cervical Two-Segments Different Internal Fixation Systems: A Finite Element Study

DAN LI[1], YUTING YU[1], DONG CHAO[2], AND QINGQING YU[3]
[1]Rail Transit Rolling Stock College, Hunan Railway Professional Technology College, Shifeng, Zhuzhou, Hunan 412001, China
[2]CRRC Zhuzhou Institute Company Ltd., Shifeng, Zhuzhou, Hunan 412001, China
[3]PKU Care Luzhong Hospital, Linzi, Zibo, Shandong 255000, China

Corresponding author: Yuting Yu (643515608@qq.com)

This work was supported in part by the Natural Science Foundation of Hunan Province under Project 2023JJ50208.

ABSTRACT One of the traditional surgical approaches for treating cervical spondylosis is anterior cervical discectomy and fusion (ACDF). The conventional titanium plate fixation method and the Zero-P internal fixation method are now the two most used anterior internal fixing techniques. Although these two fixation procedures have been clinically validated in part, their systematic theoretical analysis is still insufficient, and there are several flaws in the application comparison of double-segments cervical spine. The finite element simulation approach is used in this work to perform surgical simulation and stress analysis on two internal fixation methods. Firstly, we established a finite element model of the C3-C7 segments of the lower cervical spine and completed the validity verification of the model. Secondly, a finite element model of the internal fixation surgical method between Zero-P and traditional titanium plates was established. Finally, the cervical spine mobility and the stress of the internal fixation system under different postoperative movements were calculated. The results demonstrate that following typical titanium plate surgery, there is stress concentration in the intervertebral disc endplate, but the simulation results after Zero-P surgery are rather stable. The theoretical life of Zero-P fastening screws is rather limited, and typical titanium plates are prone to fatigue failure around the nail holes. The breadth of the Zero-P cage and the fusion site modification during surgery have a direct influence on the contact between the cervical spine and the instrument following surgery, which is also a major cause of edge fatigue failure.

INDEX TERMS Anterior, decompression and fusion, double segment, finite element analysis.

I. INTRODUCTION

One of the most prevalent degenerative illnesses treated with spine surgery is cervical spondylosis. Cervical spondylosis is getting more common and younger as a result of changes in modern lifestyle and work environment [1], [2], [3], [4], [5]. Cervical spondylosis is a condition caused by cervical spinal cord and nerve compression due to intervertebral disc protrusion and ligament hypertrophy. Nerve compression is a common issue for patients with cervical spondylosis, and conservative therapy frequently falls short of expectations [6], [7], [8], [9], [10], [11], [12].

Anterior cervical discectomy and fusion (ACDF) and artificial cervial disc replacement (ACDR) are surgical operation to treat cervical disc herniation, myeloid foraminal stenosis, degenerative cervical spondylosis and other diseases [13], [14], [15]. Since 1950, anterior cervical discectomy and fusion (ACDF) has become a classic surgical procedure for treating cervical spondylosis. With a single-door-shaped micro titanium plate fixation procedure, Wang Peng's finite element study revealed that the removal of the C3 vertebral plate may successfully lessen compensatory stress in the

The associate editor coordinating the review of this manuscript and approving it for publication was Wenbing Zhao.

middle and lower regions of the cervical intervertebral disc [16], [17], [18]. But because this kind of internal fixation takes longer to complete and removes more cervical vertebral components, there may be a higher chance of problems during and after surgery [19], [20], [21].

With the backing of clinical data, Wu Jiachang's team presented tailored hybrid surgery selection based on the degree of intervertebral disc degeneration and combined application of ACDF and ACDR to preserve the mobility of the operative segments as much as feasible [22], [23], [24], [25]. The majority of research on double-level cervical spondylosis, however, focuses on clinical issues and compares several measures such as VAS (Visual Analogue Scale) score, NDI (Neck Disability Index)index, and JOA (Japanese Orthopaedic Association)score. There is a lack of systematic analysis of the mechanical theory of internal fixation and fusion systems, cages, and intervertebral discs (endplates, annulus fibrosus, and nucleus pulposus) in adjacent segments of the disease.

Commonly used methods for anterior cervical discectomy and fusion (ACDF)include the traditional titanium plate internal fixation system and the new zero-profile implant (Zero-P) fusion internal fixation system. In order to gather data for the Low-P type internal fixation system's clinical research, Wang Qiang compared the effects of the Zero-P type and the new Low-P anterior cervical interbody fusion system on the biomechanics of nearby cervical spine segments. He also performed a stress analysis on the internal fixation system. However, a comparison of the benefits and drawbacks of the two low-notch fixation techniques and the conventional ACDF has not yet been done in the study [26], [27], [28]. Li Xin-Feng used the finite element method to compare the postoperative mechanical effects of single-segment decompression and fusion of the anterior cervical spine and decompression and fusion combined with titanium plates, and concluded that this type of combined surgery may have opposite stress effects on different segments. However, the actual cervical spine degenerative lesions are often complex, and systematic theoretical analysis of multi-segments fixation is particularly critical [29], [30], [31], [32], [33].

Norihiro Nishida's team established finite element models for posterior, anterior, and combined anterior-posterior fixation. Their research showed that the screw stress was higher in the posterior fixation model than in the combined fixation model, and the plate stress was lower in the anterior fixation model but the bone graft stress was higher compared to the combined fixation model [34]. Xiang Zhang's team conducted a biomechanical performance evaluation of the assembled joint fusion devices in single-level ACDF and compared them with the Zero-P device. The results showed that the range of motion (ROM) for the fused segments was close to zero in both models, but the motion in the unfused segment unevenly increased [35]. Tingxin Zhang et al. evaluated the clinical effectiveness of Zero-P in anterior decompression and fusion compared to cervical anterior plates. The results demonstrated that Zero-P and anterior cervical plates both achieved good postoperative outcomes for anterior decompression and fusion. Zero-P had advantages in postoperative swallowing difficulties, adjacent segment ossification, and surgical time [36]. Peng Ye's team designed an improved anterior cervical plate (ACP) based on topology optimization. Finite element analysis showed that topology optimization of the plate effectively reduced screw stress, thereby improving the stability of cervical segments during surgery. This enhanced the advantages of the internal fixation system in clinical application and biomechanical performance [37].

Based on the research of the above scholars, this study aims to establish a C3-C7 cervical spine model and focus on the C4-C5 and C5-C6 two-segments lesions. Anterior cervical disc fusion (ACDF) was performed on two-level diseased intervertebral discs, one using Zero-P system and the other using traditional titanium plate system. The goal of this study was to evaluate the stress of two distinct internal fixation systems following therapy for double-level cervical spondylosis, as well as the mobility of the cervical spine and the distribution of intervertebral disc biomechanics in neighboring disease segments.

By comparing and analyzing the stress-strain curves of intervertebral discs, the study examines the biomechanical characteristics of two-segment intervertebral discs under the influence of two internal fixation methods. The impact of this research on clinical decision-making and its applicability to special cases and scenarios are discussed. By comparing the stress curves of internal fixation systems and their vulnerable sections, the study confirms the extreme working conditions and risks associated with the two internal fixation methods, and provides technical points to pay attention to and suggestions for structural improvements when using these methods.

It is anticipated that the research findings will offer theoretical reference for medical care.

II. MATERIALS AND METHODS

A. C3-C7 THREE-DIMENSIONAL FINITE ELEMENT MODEL ESTABLISHMENT

1) THREE-DIMENSIONAL MODEL ESTABLISHMENT

As seen in **Fig.** 1A, the cervical vertebral surface envelope model at the C3–C7 segments is derived using the CT scan data of a healthy individual. Using Solidworks three-dimensional modeling software, the cervical vertebra model's surface features are closed and optimized to create a three-dimensional model. The **Fig.** 1B and 1C display the models.

Import the C3-C7 three-dimensional solid model into the Hypermesh finite element software, and divide the model into finite element meshes through the 2D/3D mesh function. The specific mesh parameters are as shown in Table 1. The essential model parameters are then defined as indicated in **Fig.** 2A after the finite element mesh model. And the assembly relationship between each cone and the intervertebral disc are imported into Abaqus CAE.

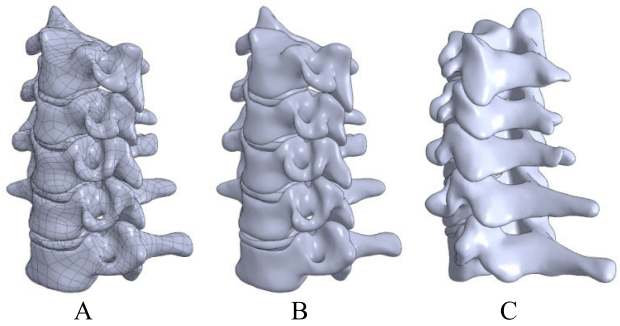

FIGURE 1. C3-C7 three-dimensional solid model. (A) 3D surface envelope model. (B) 3D solid model (front). (C) 3D solid model (rear).

TABLE 1. Grid unit types and parameters.

Component	Grid type	Total number of grids	Grid size
cortical bone	S3(triangular shell element)	24820	1mm
cancellous bone	C3D4(four-node linear tetrahedral element)	127005	1mm
end plate	C3D4	14153	1mm
annulus fibrosus	C3D4	7446	1mm
nucleus pulposus	C3D4	4569	1mm

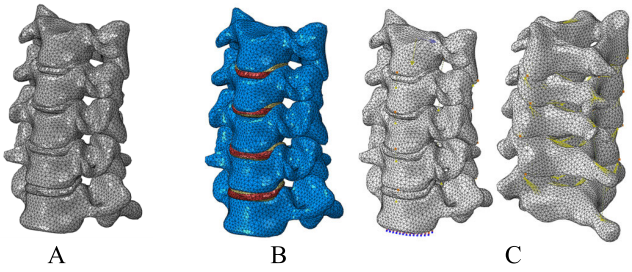

FIGURE 2. C3-C7 finite element model. (A) Finite element mesh model. (B) Material property assignment model. (C) Interaction and boundary definition model.

2) MATERIALS AND PROPERTIES

According to the relevant parameters in Table 2, the material properties are assigned to the C3-C7 finite element mesh as shown in Fig. 2B.

In the finite element model of the entire C3-C7 segments, the interactive relationships include the following locations: the intervertebral disc and the upper and lower vertebral bodies, the internal interface of the intervertebral disc, the articular processes of the upper and lower adjacent segment pyramids, and the anterior longitudinal ligament, posterior longitudinal ligament, ligamentum flavum, interspinous ligament, and capsular ligament.

Between the intervertebral disc and the upper and lower vertebral bodies, binding constraints are established to simulate the tight connection between the annulus fibrosus and the vertebral body. The interior of the intervertebral disc is refined into upper and lower endplates, nucleus pulposus, and annulus fibrosus, and binding constraints are used between each part. Establish an overall interaction model of the intervertebral disc. Possible contact attributes are established between the articular processes of the upper and lower adjacent segment cones, and are simulated by defining frictionless sliding pairs, forming a total of 8 pairs of contact combinations.

TABLE 2. Mechanical properties of materials used in cervical spine models.

Material type	Elastic Modulus（MPa）	Poisson's ratio
ortical bone	12000	0.29
cancellous bone	100	0.29
End plate	500	0.4
annulus fibrosus	3.4	0.4
nucleus pulposus	1	0.49
cartilage	10.4	0.4
anterior longitudinal ligament	30	0.3
posterior longitudinal ligament	20	0.3
ligamentum flavum	1.5	0.3
interspinous ligament	1.5	0.3
capsular ligament	100	0.3
bone graft block	100	0.29
titanium plate screws (titanium alloy)	114000	0.35
fusion	3400	0.4

Since ligaments are fibrous tissues and can only bear tensile loads under loading conditions, linear elements with only tension characteristics are used. Reference points at corresponding positions are set on the front and rear sides of the vertebral body, between adjacent laminae, and between each spinous process and the end of the spinous process, and are associated with the ligament nodes in the corresponding areas through motion coupling. The simulation of the structure and motion form of five groups of ligaments is realized by connecting the reference points and the ligament attachment locations they represent with the help of the connection unit. Refer to the material properties of each part of the ligaments in Table 2, assign cross-sectional attributes to the connection unit, and complete the establishment of the finite element model of the ligament as shown in **Fig.** 2C.

3) BOUNDARY AND LOAD

Taking normal adult human neck movements as a reference, an equivalent head gravity surface load of 73.6N is applied to the upper surface in the C3 segment. At the same time, several neck movements such as forward flexion, back extension, side bending and rotation are simulated by setting a 1N.m

bending moment with each motion axis as the center of rotation. A complete fixed constraint is applied to the lower surface of the C7 vertebral body to equivalently simulate the relative motion between C7 and the following segments. The completed load model is shown in **Fig.** 2C.

B. ESTABLISHMENT OF THE THREE-SEGMENTS FUSION MODEL OF TRADITIONAL ANTERIOR INTERNAL FIXATION

Cervical curvature is crucial for maintaining a normal cervical axis and cervical balance stability. The cervical spine internal fixation devices in this study are suitable for degenerative diseases, unstable cervical spine, and spondylolisthesis. Anterior cervical fixation surgery is highly recommended by clinical orthopedic surgeons due to its advantages such as sufficient decompression, restoration of normal physiological curvature of the cervical spine, and high fusion rate. It restores the physiological anterior convexity and intervertebral height of the cervical spine through methods such as interbody replacement, bone fusion, and anterior fixation. This is important for relieving spinal cord tension, protecting spinal cord function, and improving postoperative neurological function. In recent years, with the continuous application and improvement of anterior cervical plates and the Zero-P method, the fusion rate has also greatly improved.

1) ESTABLISHMENT OF THREE-DIMENSIONAL PLANT MODEL IN TRADITIONAL FRONT PATH

Taking the titanium plate kit for anterior cervical internal fixation from Changzhou Huasen Medical Devices Co. Ltd. as a prototype, Solidworks was used to complete the establishment of an approximate three-dimensional model, as shown in **Fig.** 3D. The specific models and parameters selected are listed in Table 3. In this context, the numerical representation of ''Type'' signifies the product series (e.g., 11.111), component number (e.g., .01), and length identifier (e.g., −053).

This set of cervical spine internal fixation devices is suitable for instability and slippage of the cervical spine caused by trauma, degenerative disease, spinal stenosis, and fusion failure. For cervical spine instability and slippage brought on by trauma, degenerative disease, spinal stenosis, and fusion failure, this set of internal fixation devices for the cervical spine is appropriate. In order to more accurately replicate the relationship between the anterior cervical spine and the postoperative internal fixation system, the titanium plate model keeps the instrument prototype's low incision features and anatomical arc design.

2) ESTABLISHING A MODEL AFTER TRADITIONAL ANTERIOR INTERNAL FIXATION USING C4-C6 AS FUSION SEGMENTS

Taking C4, C5, and C6 as the target fusion segments, the established three-dimensional model of the cervical spine anterior internal fixation titanium plate kit was used for implantation simulation. At C4, C5, and C6, respectively, intervertebral discs were extracted. A low incision was made to treat the anterior cervical implantation entry, and fusion cages and bone grafts were inserted. The anterior cervical spine titanium plate type I (11.111.01-053) was utilized to complete the connection and fixation after six anterior cervical spine screws (11.111.02-616) were used to pierce the preselected sites on the front of the C4, C5, and C6 cones. Make that the target cone's physical range is accommodated by the specified screw insertion angle and length specifications. At the same time, the anatomical arc connecting the titanium plate should be basically consistent with the physiological arc of the anterior side of the C4-C6 cone to reduce the risk of interference in the model. The established model after anterior decompression and fusion is shown in Fig. 4A and 4B.

Referring to the grid unit types and parameter settings of each component in Table 1, combined with the parameter settings of the C3D4 unit of the traditional internal fixation kit, the division of the finite element grid was completed, and a total of 824,582 grids were generated. Complete the relevant assignments of the finite element model according to the material and cross-sectional properties in Table 2. Refer to the simulation of boundary conditions and loads in Chapter II-A. Taking the normal adult human neck movement as a reference, an equivalent head load of 73.6N is applied. Under

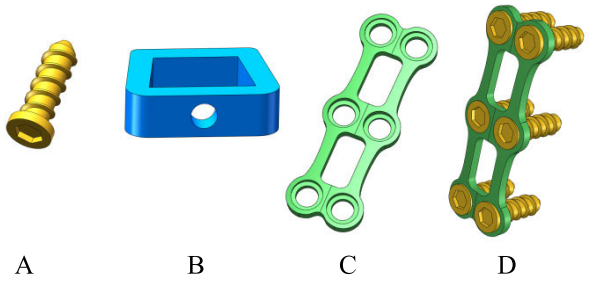

FIGURE 3. Three-dimensional model of anterior cervical spine internal fixation. (A) Anterior cervical screw. (B) Cage. (C) Anterior cervical spine titanium plate type I. (D) Anterior cervical spine internal fixation assembly.

TABLE 3. Parameters of anterior cervical spine internal fixation.

Device name	Type	Length(mm)	Parameter 1(mm)	Parameter 2(mm)
anterior cervical spine titanium plate type I	11.111.01-053	53	Width18	thickness2.1
anterior cervical screw	11.111.02-616	16	diameter4	-
cage	11.616.21-005	11	Width14	height5
Device name	Type	Length(mm)	Parameter 1(mm)	Parameter 2(mm)
anterior cervical spine titanium plate type I	11.111.01-053	53	Width18	thickness2.1

the action load of 1N.m bending moment, the lower surface of the C7 vertebral body is completely fixed. The established finite element model is shown in Fig. 4C.

Corresponding settings are created for the three-segments conventional anterior internal fixed finite element model, with reference to the approach used to develop the interaction connection between the C3-C7 segments in Chapter II-A. In addition, the model also includes the threaded connection formed between 6 fixation screws and vertebral bodies, and the connection between the screw and the connecting titanium plate, and the three pairs of contact areas formed between the titanium plate and the front side of the C4-C6 three-segments vertebral body.

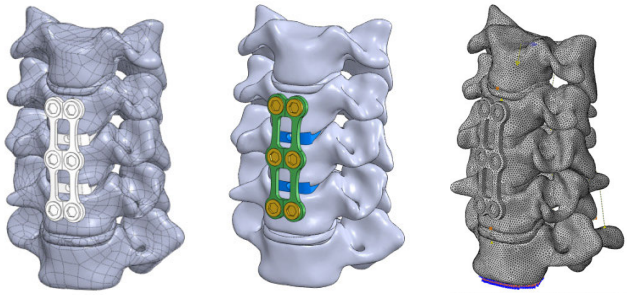

FIGURE 4. Model after anterior decompression and fusion. (A) 3D surface envelope mode. (B) 3D solid mode. (C) Finite element model.

C. ESTABLISH A THREE-SEGMENTS FUSION MODEL OF ZERO-P ANTERIOR INTERNAL FIXATION

1) ESTABLISHMENT OF THREE-DIMENSIONAL MODEL OF PLANTS IN ZERO-P

Taking the anterior cervical zero-p internal fixation kit from Beijing Zhongan Taihua Technology Co., Ltd. as a prototype, 3D software was used to complete the establishment of an approximate three-dimensional model, as shown in the Fig. 2D. The specific selected models and parameters are listed in Table 4. This set of cervical spine internal fixation devices is suitable for degenerative diseases, spinal stenosis, unstable cervical spine and spondylolisthesis. The bone grafting area of the kit is large, which is conducive to postoperative fusion. The four screws are locked and connected to the fixation plate, which can effectively reduce the risk of screw withdrawal; and the zero-p design reduces the risk of dysphagia. The three-dimensional model retains the edge curvature characteristics of the device prototype, and adopts a wedge-shaped area screw insertion method with a screw head and tail end angle of $40°\pm5°$ and a medial and lateral angle of 2.5° to more realistically restore the biomechanical characteristics of the postoperative fixation system.

2) USING C4-C6 AS FUSION SEGMENTS TO ESTABLISH A MODEL AFTER ZERO-P ANTERIOR INTERNAL FIXATION

The C4, C5, and C6 segments were employed as the target fusion segments, and the developed three-dimensional model

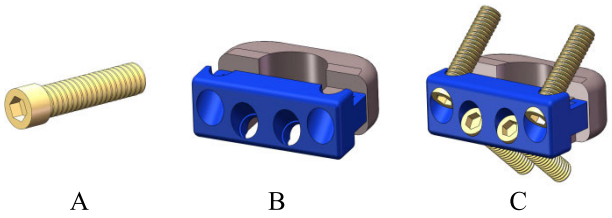

FIGURE 5. Three-dimensional model of anterior cervical spine Zero-P internal fixation. (A) Locking screw. (B) Zero-P Cage. (C) Anterior cervical spine internal fixation assembly.

TABLE 4. Grid unit types and parameters.

Device name	Type	Length(mm)	Parameter 1(mm)	Parameter 2(mm)
zero Notch Cage	53090500003	13.5	Width 17.5	Thickness7
locking screw	5420100015	12	Diameter 3	-

of anterior cervical Zero-P internal fixation was used for implant simulation, with reference to the model establishment approach in Chapter II-A. Intervertebral discs were removed for C4, C5, and C6 respectively, and pre-implantation treatment was performed, and cages and bone grafts were implanted. Use 4 fixing screws (5420100015) to penetrate the C4 and C5 cones, secure the cage device firmly (53090500003), and ensure that the fixing screw insertion angle and length parameters adapt to the physical range of the target cone. Using the same technique, the C5 and C6 segments of cage insertion and fixing were finished. Fig. 6A and 6b depict the established Zero-P fusion postoperative paradigm.

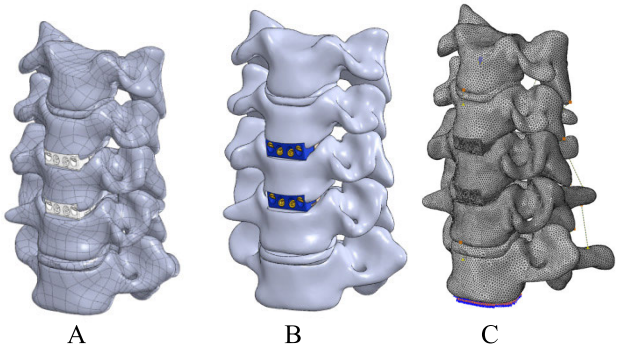

FIGURE 6. Zero-P fusion postoperative model. (A) 3D surface envelope model. (B) 3D solid model. (C) Finite element model.

According to the grid unit type and parameter settings of each component, combined with the parameter settings of the C3D4 unit of the Zero-P cage device, the division of the finite element grid was completed, and a total of 1,467,280 grids were generated. According to the material and cross-section properties in Table 2, the relevant assignments of the finite element model are completed, and the interaction relationship

and boundary load of the C3-C7 segments are completed. The established finite element model is shown in Fig. 6C.

III. RESULT

A. VALIDITY VERIFICATION OF THE MODEL

Submit the established finite element model of the C3–C7 cervical vertebrae in a typical human body, and use the Abaqus standard solver to perform finite element analysis and solution. Fig. 7 displays the cloud image findings that were computed.

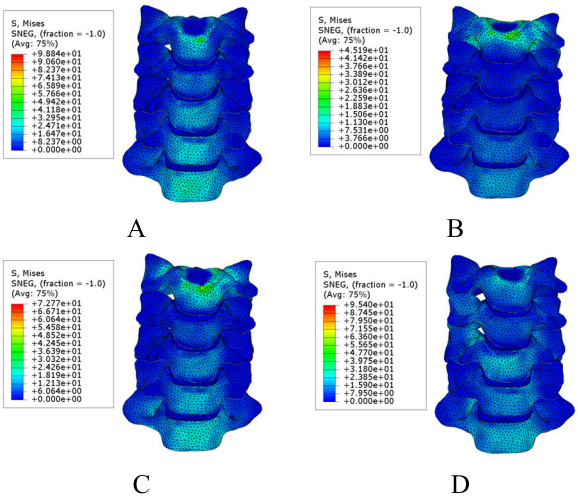

FIGURE 7. Equivalent stress (Mises) result cloud diagram of normal cervical spine at C3-C7 segments. (A) Forward bend. (B) Extension. (C) Bend. (D) Axial rotation.

According to the equivalent stress cloud diagram of the C3-C7 cervical vertebrae in the figure, Fig. 7A and 7B show that the stress on the anterior-driven vertebral body is mainly distributed in the anterior cervical area. The equivalent stress on the vertebral body during backward extension is primarily distributed in the vertebral arch and posterior cervical area on both sides, and the average stress value is smaller than that during forward movement. In addition, the average stress value of the two end segments is slightly higher than that of the middle segment. In Fig. 7C, the stress distribution of the vertebral body is generally consistent with that of forward flexion during lateral flexion movements. The difference is mainly reflected in the change in the mean stress in the left and right areas of the vertebral body corresponding to the left and right movements. In Fig. 7D, the axis rotation movements are basically consistent with the stress distribution on the lateral flexiont sides, but the average stress value is slightly larger.

Table 5 illustrates the calculation of the C3-C7 cervical intervertebral mobility ROM value based on the corner displacement data found in the finite element analysis findings.

The intervertebral mobility of the cervical spine C3-C7 finite element model established in this article was compared with the experimental data results of in vitro biomechanical measurements by Moroney [38] and Panjabi [39], and both were within the normal deviation range of mobility. The specific verification results are shown in Fig. 8. The finite element model of the normal human C3-C7 cervical vertebrae has been verified effectively.

TABLE 5. Intervertebral mobility ROM (°) of cervical spine under 1Nm load in this study.

	C3-C4	C4-C5	C5-C6	C6-C7
Flexion and extension	7.7	8.8	8.7	8.0
Lateral flexion	7.3	6.0	5.8	4.9
Axis rotation	4.4	7.6	6.0	3.8

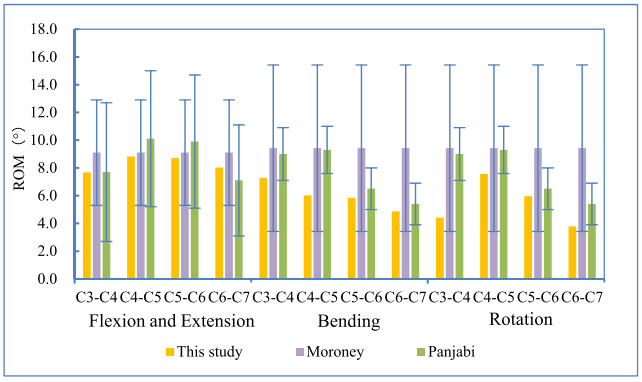

FIGURE 8. Comparison of intervertebral range of motion.

The differences between this research model and previous research models are as follows. Firstly, it primarily arises from the level of optimization of the cervical spine model, the level of reduction and simplification of the internal fixation device model. And it is also related to the degree of finite element mesh division, and the process of assigning material properties. Particularly, this study adopts an area-distributed selection method and a point-surface synchronous coupling definition method to simulate ligaments, aiming to more realistically replicate the range of ligament attachments and overall force distribution in the cervical spine based on clinical research data. Finally, the interaction properties and range settings of each finite element component can also lead to subtle differences in simulation results.

B. MOBILITY AND STRESS CONDITIONS OF THE MODEL AFTER TRADITIONAL ANTERIOR INTERNAL FIXATION OF THE C4-C6 FUSION SEGMENTS

The finite element results of the model's mobility after traditional anterior internal fixation of the C4-C6 fusion segments are shown in Fig. 9. The overall flexion and extension mobility of the cervical spine is about 7°, the lateral flexion motion is only 4°, and the axis rotation mobility is close to 8°. The average intervertebral mobility of the C3-C4 segment accounts for nearly 63.2%, which is preserved to a large

extent, but is still about 49.4% lower than the preoperative simulation results. Under each cervical vertebra movement, the overall mobility of the C4-C6 segments were around 0.6°, which was 13.5° lower than the preoperative simulation results, and its range of motion was reduced by 95%.

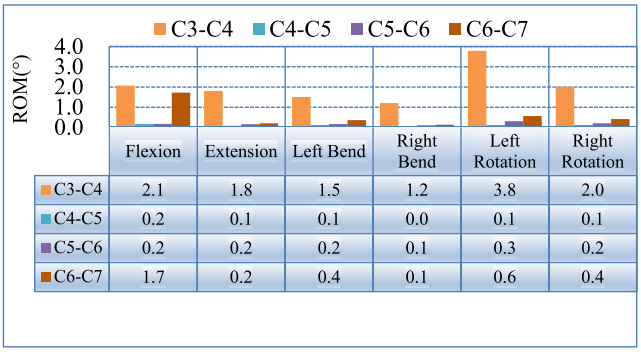

	Flexion	Extension	Left Bend	Right Bend	Left Rotation	Right Rotation
C3-C4	2.1	1.8	1.5	1.2	3.8	2.0
C4-C5	0.2	0.1	0.1	0.0	0.1	0.1
C5-C6	0.2	0.2	0.2	0.1	0.3	0.2
C6-C7	1.7	0.2	0.4	0.1	0.6	0.4

FIGURE 9. Simulation results of intervertebral range of motion after traditional anterior internal fixation of the C4-C6 fusion segments.

The finite element simulation results of traditional anterior internal fixation are shown in Fig. 10. A-D are the equivalent stress cloud diagrams under each types of cervical spine movements respectively. As can be observed, the highest equivalent stress on the cervical spine surpasses the stress value of the internal fixation system, although the average equivalent stress for each action condition is less than that stress value. This is mainly due to the stress concentration phenomenon caused by the boundary load applied to individual node positions and the contact of the vertebral facet joints. Some tips or nodes may exceed the true value, but the overall cervical spine conforms to the stress distribution trend.

Through the comparison of the data in Fig. 11, the average stress value of the internal fixation system fluctuates between 18-40 MPa under different working conditions. The stress peak occurs during the left-rotation movement, exceeding the average value of the right-bend movement by about 16.9Mpa, and the excess ratio is about 46.3%. The internal fixation system's greatest stress value, which accounts for around 55.1% of the stress, is 87.5 Mpa during the left-rotation movement, exceeding the maximum value of 48.2 Mpa during the right-bend movement. During the right- rotation, both the average stress and the maximum stress are at the second peak value, which is slightly greater than that of the flexion, extension, and left bend. Similarly, the average stress value of the cervical spine fluctuates between 1-3.5 MPa under different working conditions, and the peak value also occurs during left-rotation movements, exceeding the average value of right-bend movements by 1.5 MPa. The maximum stress value of the cervical vertebra appears at about 102.2Mpa during the left rotation. There is an obvious stress concentration phenomenon. It exceeds the second peak value of 20.1Mpa during the right rotation, and the excess ratio is about 19.7%. The average stress of other flexion, extension and bend movements fluctuates within the 3Mpa range, and the changes in the maximum stress are basically the same.

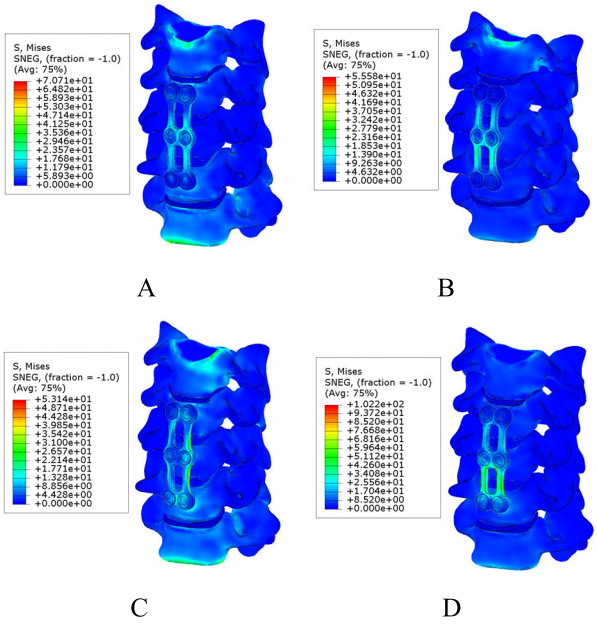

FIGURE 10. Finite element equivalent stress (Mises) cloud diagram of traditional anterior internal fixation of C4-C6 fusion segments. (A) Forward bend. (B) Extension. (C) Bend. (D) Axial rotation.

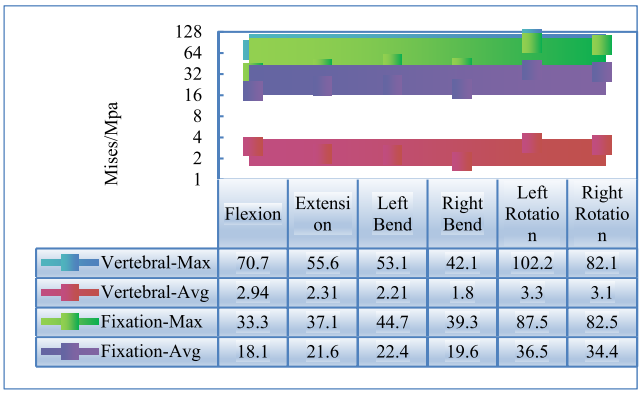

	Flexion	Extension	Left Bend	Right Bend	Left Rotation	Right Rotation
Vertebral-Max	70.7	55.6	53.1	42.1	102.2	82.1
Vertebral-Avg	2.94	2.31	2.21	1.8	3.3	3.1
Fixation-Max	33.3	37.1	44.7	39.3	87.5	82.5
Fixation-Avg	18.1	21.6	22.4	19.6	36.5	34.4

FIGURE 11. Comparison curve of equivalent stress values between vertebral body and traditional internal fixation system.

Fig. 12-13 displays the comparable stress cloud diagram findings of the intervertebral disc following conventional anterior internal fixation, using C4-C6 as the fusion level. It can be seen from the cloud image that the equivalent stress value on the upper and lower endplates of the intervertebral disc is significantly greater than that of other parts, and there is a trend that the edge stress is greater than the center stress. This is related to the characteristics of the arc surfaces at both ends, and some movements also cause local stress concentration. The minimum value of stress appears in the nucleus pulposus, and its stress distribution range basically shows a tendency that the middle area is slightly larger than the periphery. The specific distribution is related to the different working conditions of the cervical spine. The stress in the annulus fibrosus is between the end plate and the nucleus pulposus, and its stress distribution is relatively uniform.

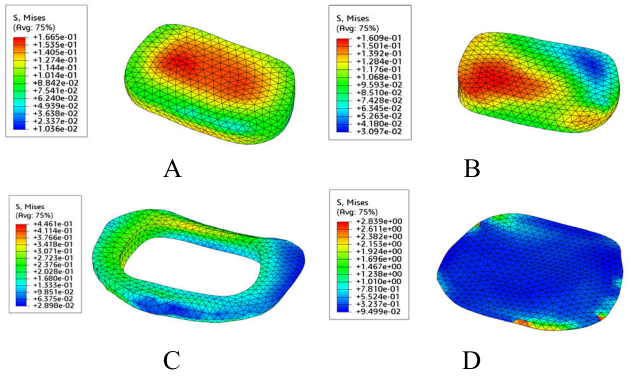

FIGURE 12. Equivalent stress cloud diagram of C3-C4 intervertebral disc after traditional anterior internal fixation. (A) Stress cloud diagram of nucleus pulposus during flexion. (B) Stress cloud diagram of nucleus pulposus during axial rotation. (C) Stress cloud diagram of annulus fibrosus during bending action. (D) Stress cloud diagram of endplate during bending action.

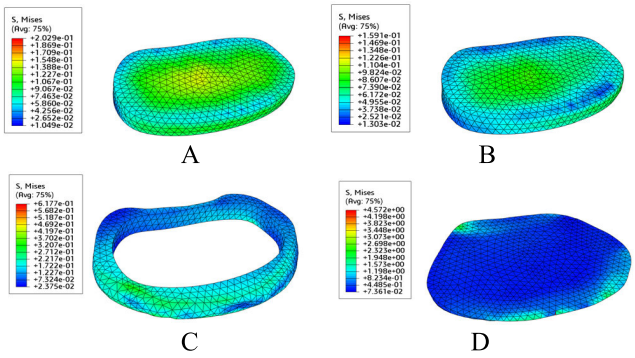

FIGURE 13. Equivalent stress cloud diagram of C6-C7 intervertebral disc after traditional anterior internal fixation. (A) Stress cloud diagram of nucleus pulposus during flexion. (B) Stress cloud diagram of nucleus pulposus during axial rotation. (C) Stress cloud diagram of annulus fibrosus during bending action. (D) Stress cloud diagram of endplate during bending action.

The stress concentration in some areas is also related to the specific cervical spine movements.

In Fig. 14, internal bone graft 1 and internal bone graft 2 are respectively located between the C4-C5 and C5-C6 segments of traditional internal fixation. The equivalent stress of bone grafting is larger at the edge than at the center, similar to the upper and lower endplates. Its stress value is smaller than the corresponding situation of the endplate. And with the change of cervical spine movement, the concentration of stress on the edge of the bone graft also shows different distribution patterns. This circumstance is also closely connected to the stress of the cage device, according to a comparison of the cage stress result cloud diagram.

Cage 1 and cage 2 are respectively located between the C4-C5 and C5-C6 segments of traditional internal fixation. The stress magnitude and distribution on the inside of the cage are basically the same as the internal bone grafting conditions, while the stress on the outside is mainly caused by the compression and relative shear force between the upper

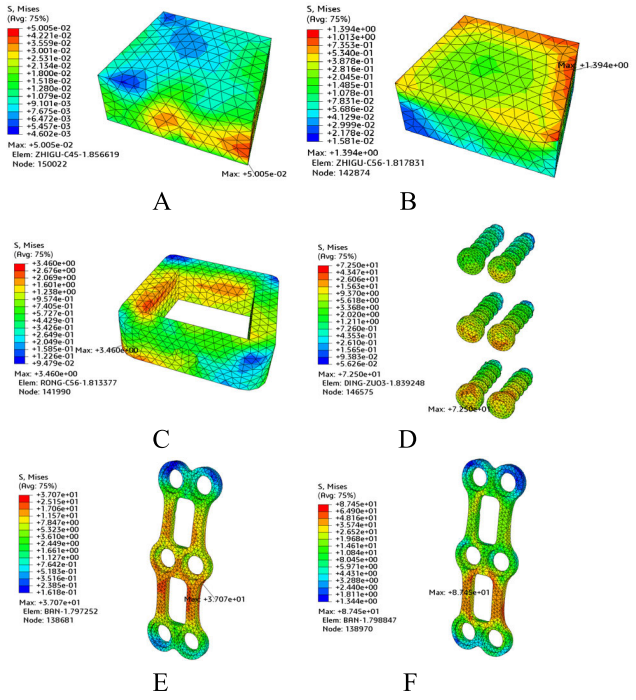

FIGURE 14. Equivalent stress cloud diagram of C4-C6 internal fixation system after traditional anterior internal fixation. (A) Stress cloud diagram of internal bone graft 1 during bend action. (B) Stress cloud diagram of internal bone graft 2 during bend action. (C) Stress cloud diagram of cage during axial rotation. (D) Stress cloud diagram of screws during rotational action. (E) Stress cloud diagram of titanium plate during flexion and extension movements. (F) Stress cloud diagram of titanium plate during axial rotation.

and lower vertebrae. Its maximal value, in contrast, is less than the concentrated stress produced at the intervertebral disc endplate's edge.

In Fig. 14, the forces on traditional internal fixation screws and titanium plates are strongly related to cervical spine movements, and their stress peak points appear at the left 3 screw connections during axial rotation.

There is a clear stress concentration distribution in the middle link area when the titanium plate flexes and extends. During the axial rotation operation, the largest stress peak occurs at the lower link location.

C. THE MOBILITY AND STRESS OF THE MODEL AFTER C4-C6 FUSION SEGMENTS ZERO-P ANTERIOR INTERNAL FIXATION

The limited range of motion of the model after Zero-P internal fixation of the C4-C6 fusion segments is shown in Fig. 15. The cervical spine has an overall flexion and extension mobility of around 13.8°, a bend motion of just 9.1°, and an axial rotation mobility of almost 18.3°. Among them, the average proportion of intervertebral mobility of the C3-C4 segment is close to 61.8%, which is basically consistent with the average value of the preoperative simulation results. The mobility is only reduced during bend motion. The C4-C6 segments' total mobility under each cervical vertebral movement was around

1°, which was 13.1° less than the preoperative simulation findings, and its range of motion was 92% less.

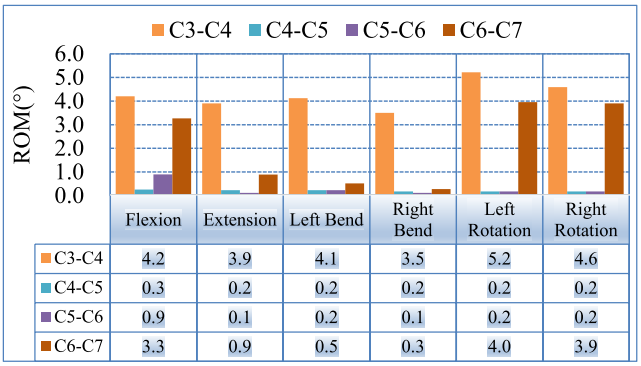

	Flexion	Extension	Left Bend	Right Bend	Left Rotation	Right Rotation
C3-C4	4.2	3.9	4.1	3.5	5.2	4.6
C4-C5	0.3	0.2	0.2	0.2	0.2	0.2
C5-C6	0.9	0.1	0.2	0.1	0.2	0.2
C6-C7	3.3	0.9	0.5	0.3	4.0	3.9

FIGURE 15. Simulation findings of C4-C6 fusion segments range of motion following Zero-P internal fixation.

The finite element simulation results after Zero-P internal fixation are shown in Fig. 16. A-C are the equivalent stress cloud diagrams under each types of cervical spine movements. It is evident that, for any action situation, the corresponding stress on the cervical spine body is smaller than the stress value of the internal fixation system.

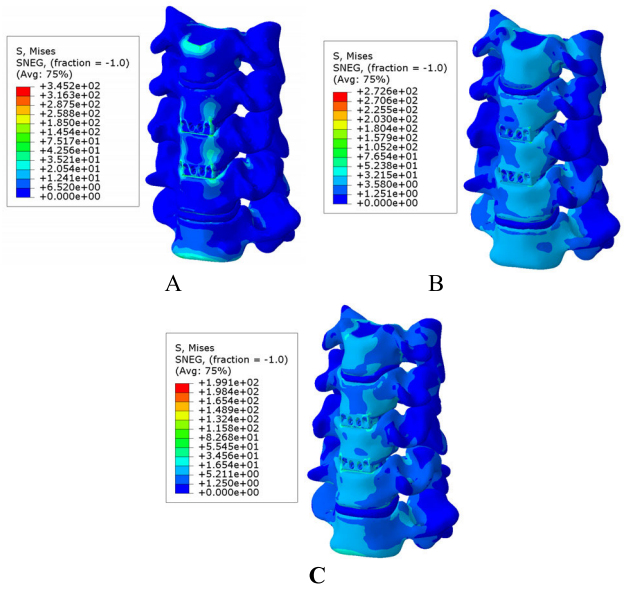

FIGURE 16. Finite element equivalent stress cloud diagram of Zero-P internal fixation system for C4-C6 fusion segments. (A) Flexion and extension. (B) Bend motion. (C) Axial rotation.

The average stress value of the internal fixation system varies between 4 and 12 MPa under various operating situations, as can be seen by comparing the data in Fig. 17. The stress peak happens during the flexion movement, surpassing the percentage by approximately 62.3% and the average value of the extension action by around 7.17 Mpa. The maximum stress value of the internal fixation system is 345Mpa during flexion, which is mainly distributed in the edge area. There is an obvious stress concentration phenomenon. It exceeds the maximum value of 265Mpa during backward extension, accounting for about 76.8% of the stress. The average stress and maximum stress during the right-rotation are both at the second peak, which is marginally higher than during the bend motion and left-rotation. Similar to this, the average stress value of the cervical spine varies between 0.5 and 5 Mpa depending on the working environment. It peaks during flexion motion is 4 Mpa higher than the average value of extension motion. The maximum stress value of the cervical spine appears at about 116.8Mpa in the flexion, exceeding the second peak of 54Mpa in the extension, and the excess ratio is about 46.2%. The average stress of the remaining bend motion and axial rotation fluctuates within the 3Mpa range, and the changes in the maximum stress are basically the same.

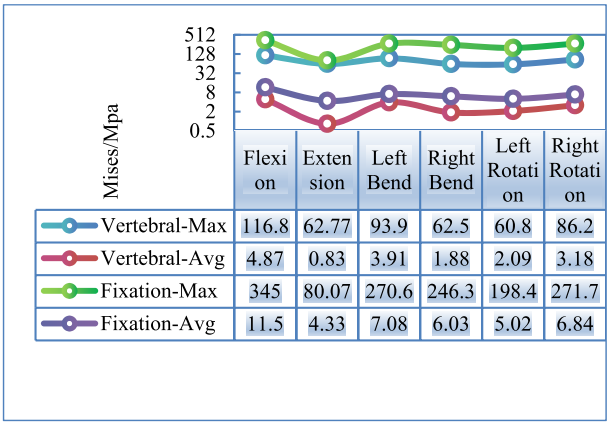

	Flexion	Extension	Left Bend	Right Bend	Left Rotation	Right Rotation
Vertebral-Max	116.8	62.77	93.9	62.5	60.8	86.2
Vertebral-Avg	4.87	0.83	3.91	1.88	2.09	3.18
Fixation-Max	345	80.07	270.6	246.3	198.4	271.7
Fixation-Avg	11.5	4.33	7.08	6.03	5.02	6.84

FIGURE 17. Comparison curve of equivalent stress values between vertebral body and Zero-P internal fixation system.

The equivalent stress cloud diagram results of the intervertebral disc after Zero-P internal fixation with C4-C6 as the fusion level are shown in Fig. 18-19. The cloud image results show that the performance of the intervertebral disc after traditional internal fixation is basically consistent. Both the top and lower endplates have bigger equivalent stress values, and the margins have greater stress than the centre. At the boundaries, there is also a concentration of stress. The stress in the nucleus pulposus is small, and the stress in the annulus fibrosus is between the end plate and the nucleus pulposus. The stress concentration in all areas is related to the movement of the cervical spine.

In Fig. 20, internal bone graft 3 and internal bone graft 4 are respectively located between the C4-C5 and C5-C6 segments of Zero-P internal fixation. The equivalent stress of the bone graft is related to the movement of the cervical spine. As the working conditions change, the stress concentration area shifts significantly, and its stress value is smaller than that of the end plate, nucleus pulposus, and annulus fibrosus.

Cage 3 and cage 4 are respectively located between the C4-C5 and C5-C6 segments of Zero-P internal fixation. In the

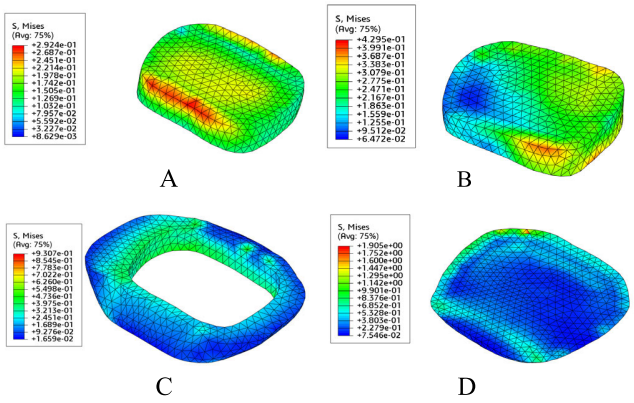

FIGURE 18. Equivalent stress cloud diagram of C3-C4 intervertebral disc after Zero-P internal fixation. (A) Stress cloud diagram of nucleus pulposus during flexion. (B) Stress cloud diagram of nucleus pulposus during axial rotation. (C) Stress cloud diagram of annulus fibrosus during bend action. (D) Stress cloud diagram of endplate during bend action.

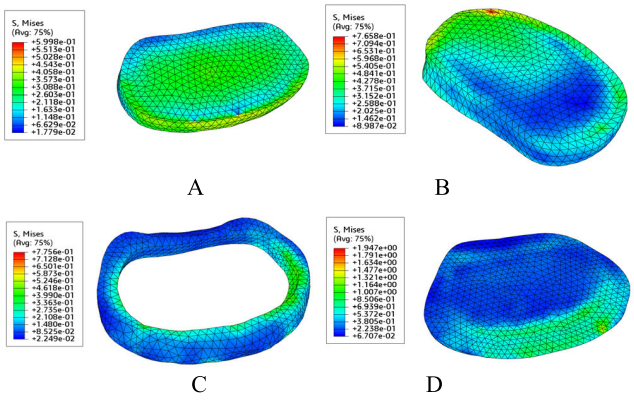

FIGURE 19. Equivalent stress cloud diagram of C6-C7 disc after Zero-P internal fixation. (A) Stress cloud diagram of nucleus pulposus during flexion. (B) Stress cloud diagram of nucleus pulposus during axial rotation. (C) Stress cloud diagram of annulus fibrosus during bending action. (D) Stress cloud diagram of endplate during bending action.

early stages of establishing the three-dimensional model, considering possible edge stress conditions, the cage retained the arc design of the device prototype, which can unload and optimize stress distribution to a certain extent. However, compared with traditional cages, the cage used by Zero-P does not have an anterior support and fixation similar to a titanium plate connecting rod. Instead, it completely relies on the support surface of the cage itself for force transmission and action. Under various motion conditions of the cervical spine, concentrated loads will inevitably occur at the edge positions, resulting in stress concentration in a small area, such as the top corner area of the cage as shown in the figure.

The stress of the Zero-P internal fixation screw is closely related to cervical spine movement, and its maximum stress value point will fluctuate as working conditions change. During the flexion and extension action, the maximum stress value of screw appears at the head connection of the second screw on the left (left 2). The stress peak appears at the head of

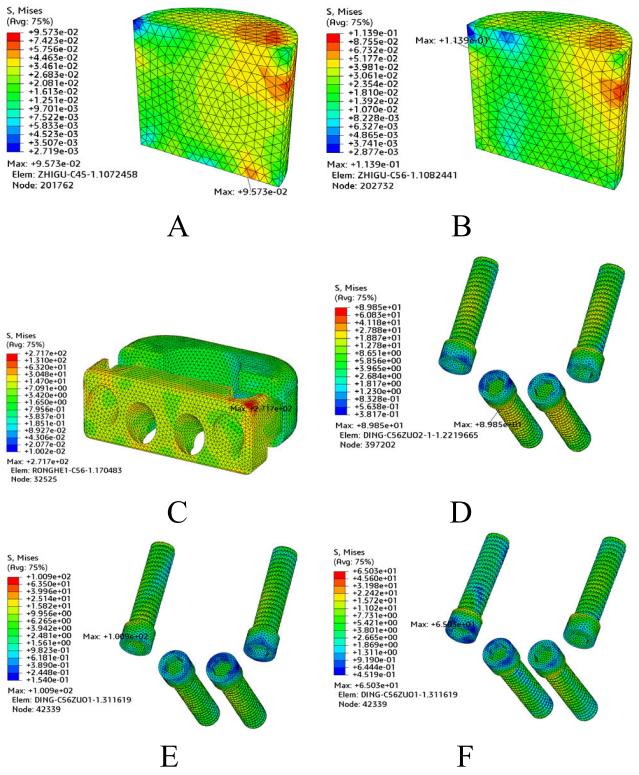

FIGURE 20. Equivalent stress cloud diagram of the C4-C6 internal fixation system after Zero-P internal fixation. (A) Stress cloud diagram of internal bone graft 1 during bend action. (B) Stress cloud diagram of internal bone graft 2 during bend action. (C) Stress cloud diagram of cage during axial rotation. (D) Stress cloud diagram of screws during flexion and extension movements. (E) Stress cloud diagram of screw during bend action. (F) Stress cloud diagram of screws during axial rotation.

the left 1 screw while bend action. The stress peak emerges at the connection between the left 1 screws while axial rotation.

IV. DISCUSSION

A. COMPARATIVE ANALYSIS OF INTERVERTEBRAL DISC STRESS VALUE CURVES

The postoperative equivalent stress comparison curves of the two internal fixation methods are shown in Fig. 21 and 22. It can be seen that the maximum stress value of the end plate of both methods exceeds the corresponding value of the nucleus pulposus and annulus fibrosus, and the maximum stress value of the end plate of the traditional method reaches about 12.5Mpa during right rotation, which is greater than the end plate of the Zero-P method. The corresponding value is about 8Mpa, accounting for 36%. The stress on the nucleus pulposus of the two internal fixation methods is relatively uniform. The traditional method basically remains between 0.2-0.4Mpa, but the maximum stress of the nucleus pulposus of Zero-P rises to between 0.4-0.8Mpa. The stress level of the latter has increased significantly whether from the maximum value or the average value.

To sum up the discussion above, only considering of the stress on the nucleus pulposus, the traditional postoperative

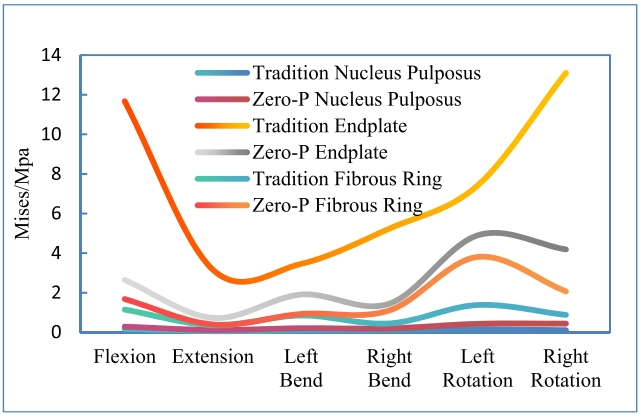

FIGURE 21. Comparison of the maximum stress value curves of the C3-C4 segment intervertebral disc.

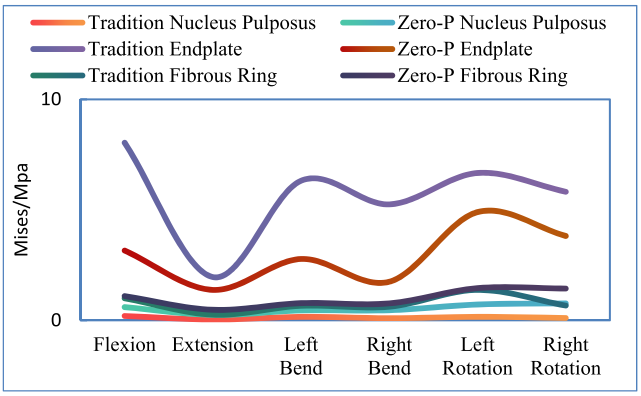

FIGURE 22. Comparison of the maximum stress value curves of the C6-C7 segment intervertebral disc.

force has less impact on the two-segments nucleus pulposus, but there is stress concentration in the endplate structure. The theoretical value determines that there is a risk of continued wear and aging in the later stages of postoperative use. In Zero-P, the overall stress level at the end plate became stable, and there was no obvious stress concentration. The postoperative simulation results were relatively stable and good.

By quantitatively analyzing the adjacent segment displacement after a Zero-P cervical fusion procedure, it is evident that there is a significant increase in the mobility of the superior adjacent segments of the fusion site. This implies that patients can compensate to some extent for the loss of cervical mobility caused by the surgery. And it can provide guidance for preoperative target setting and postoperative mobility outcomes. By comparing the stress between two internal fixation systems, the fixation strength of the Zero-P system is lower than that of the traditional anterior cervical plate fixation. From the simulation results, it can be inferred that this difference in fixation strength may be due to the shorter ''lever arm'' of the Zero-p interbody fusion device compared to the traditional anterior cervical plate system. At the same time, there is an increase in intervertebral disc pressure at the superior level of the fusion site, but there is no significant change in disc pressure at the inferior level. Additionally, the traditional anterior approach has a slightly greater impact on the intervertebral discs compared to the Zero-P approach. This indicates that in clinical treatment, the choice of internal fixation should be based not only on the analysis of the affected segments, but also on the comprehensive assessment of the intervertebral disc condition at the adjacent segments.

Based on this study and previous research, the two-level Zero-P cervical fusion is a safe and effective treatment method. The advantages of Zero-P over the traditional anterior cervical plate fixation system are in terms of operation time, blood loss, fluoroscopy times, and postoperative dysphagia rate. For patients with clear notes regarding operation time, blood loss, and dysphagia rate, the Zero-P internal fixation procedure can be considered. However, the traditional anterior cervical plate fixation system is better at reconstructing the overall cervical curvature and the curvature of the operative segments compared to the Zero-P interbody fusion device. For patients with obvious abnormal cervical curvature before surgery, such as cervical lordosis deformity, the use of the Zero-P interbody fusion device as an internal fixation device is not recommended. In addition, the screw insertion length of the Zero-P system is significantly shorter than the traditional method, so there is a higher risk of screw pullout and fusion device displacement for elderly patients with osteoporosis.

B. COMPARATIVE ANALYSIS OF STRESS CURVES OF INTERNAL FIXATION SYSTEMS

The comparison of the screw stress curves of the two internal fixation systems are shown in Fig. 23. It can be seen that under various motion conditions of the cervical spine, both the maximum and average stress values of the Zero-P method are significantly higher than those of the traditional method. Under flexion, extension and bend movements, the maximum value of the Zero-P method screw exceeds the traditional method by about 57.3% on average, and the stress value of the axial rotation is not much different. While the average stress value of Zero-P screws is around 3-6 Mpa, the average stress value of traditional fixation screws is essentially maintained at 1-2 Mpa.

As discussed above, if we only discuss the stress conditions of internal fixation screws after surgery, the maximum stress of both internal fixation screws is within the allowable range and can meet the needs of use. However, considering that the internal fixation system is accompanied by the patient's long-term use, there is an inevitable risk of aging and fatigue. Based on this degree of study, the Zero-P fixing screw's extreme value of cycle stress is almost doubled, and theoretically, its service life will be less than that of the conventional approach.

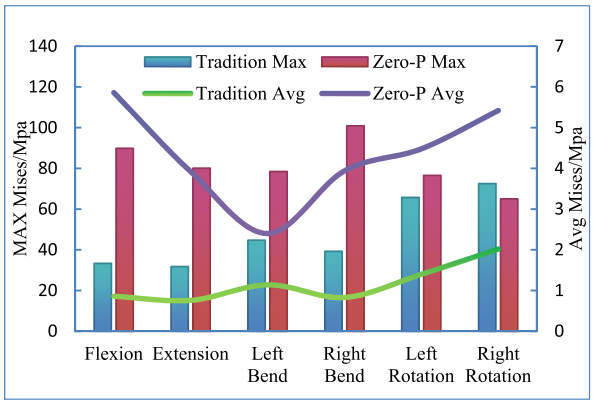

FIGURE 23. Comparison of stress value curves of two types of internal fixation screws.

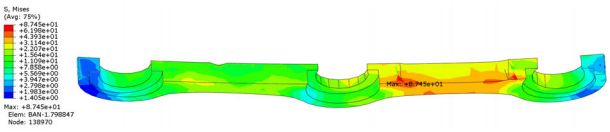

FIGURE 24. Stress cross-sectional view of the risk parts of the traditional titanium plate.

C. COMPARATIVE ANALYSIS OF CROSS-SECTION STRESS CURVES AT RISK LOCATIONS

Fig. 24 shows a cross-sectional view of the risk parts of the traditional titanium plate. It occurs during traditional postoperative left rotation of the neck, with the maximum stress value reaching 87.45Mpa. The specific risk location is the arc-shaped connecting plate between the two nail holes of the titanium plate at the C5-C6 segment. The curve in Fig. 25 shows the corresponding working conditions and cross-section in Fig. 27. On the node path along the risk section of the titanium plate, there are two stress concentrations between 40mm and 55mm, and the simulation stress results both reach about 80Mpa. The stress at the 0-30mm and 60-70mm positions is relatively average. Therefore, the risk site of the traditional titanium plate is the connecting plate corresponding to the nail hole of the C5-C6 segment, and attention should be paid to the risk of postoperative slippage and fatigue failure of the titanium plate caused by axial rotation movements.

The contact stress cloud diagrams between the titanium plate and the anterior vertebral body during different neck movements are shown in Fig. 26. As can be observed, the contact area essentially has an oval form. According to the theoretical analysis of contact mechanics, the contact belongs to the standard point contact model, and there is a definite relationship between the contact radius and the contact stress. Given that the model was established with consideration for the curvature problem of the bionic fit of the titanium plate, the contact area that appears in the contact stress data may be interpreted as potential postoperative concerns, such as mismatch in instrument selection or installation interference.

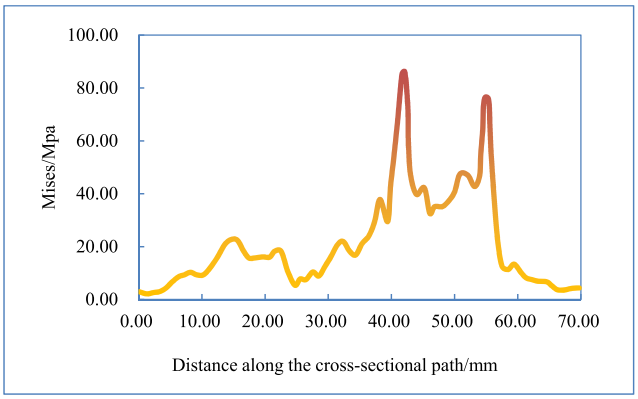

FIGURE 25. Stress curve along the cross-sectional path of traditional titanium plate.

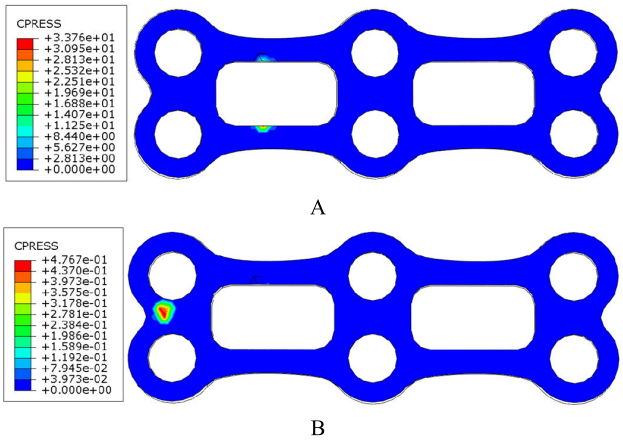

FIGURE 26. Contact stress cloud diagram of traditional titanium plate. (A) Flexion and extension. (B) Bend motion.

In the simulation results, the maximum contact stress value caused by the fit of the titanium plate and the cervical spine is 33.76Mpa during extension motion. According to the simulation, attention should be paid to the reserved installation distance and fit between the titanium plate and the segments, as well as the impact of postoperative patient extension motion on the vertebrae and titanium plate.

The stress cross-sectional image of the Zero-P cage's risk area (C5-C6 segment) is displayed in Fig. 27. It occurs during flexion motion after Zero-P surgery. The maximum stress value area is located at the contact point between the top of the right side of the cage and the vertebral body, showing obvious stress concentration. The stress value near the nail hole is only about 20Mpa, and the minimum value appears in the middle of the cage device, with a value of 1.48Mpa. The entire component has obvious uneven stress distribution and concentration.

The curve in Fig. 28 shows the working conditions and cross-section corresponding to Fig. 27. Two stress concentrations happened at the 15 mm and 20 mm positions on the node path along the cage device's risk section, and the simulation stress results for both locations reached roughly 300 Mpa.

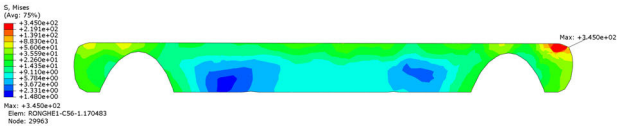

FIGURE 27. Stress cross-sectional view of the risk area of Zero-P cage.

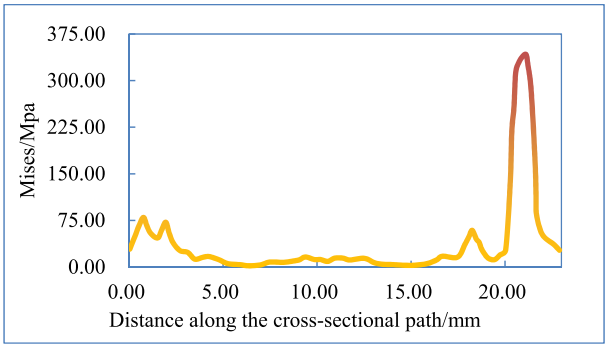

FIGURE 28. Stress curve along the cross-sectional path of the Zero-P cage.

The possibility of singular point contact in the model cannot be ruled out. However, comparing the stress value of 80Mpa at the 0-5mm position of the path (the symmetrical side), it can be preliminarily inferred that the stress concentration value should be at least greater than 80Mpa, which belongs to the risk section of the cage. According to the simulation results, the width and size parameters of the cage have a greater impact on the stress on the vertebrae after surgery, and the modification effect of the vertebral body fixation surface after intervertebral disc removal also has a direct impact on the interaction force between the vertebrae and the instrument. The cage's edge stress effect may cause fatigue failure later on, putting the vertebral body's corresponding contact point at danger of premature wear.

In terms of model fidelity and simulation accuracy, this study may have the following limitations. Firstly, the cervical spine prototype used in this study represents a normal cervical structure and does not include degenerative changes related to the cervical spine. Therefore, the representativeness of the model is limited. Secondly, the model did not include parameters related to muscle tissue, and the cervical spine-related muscles were not simulated. Additionally, all structures were represented using isotropic materials, which may differ from the actual structures. Thirdly, the results of this study were obtained through finite element analysis, and further biomechanical experiments using in vitro specimens are still needed for basic validation, along with effective clinical evidence.

V. CONCLUSION

After standard surgery, the C3-C4 segment's intervertebral motion has been mostly conserved, however it is nevertheless decreased by roughly 49.4% when compared to the results of the preoperative simulation. The C4-C6 section has a 95% reduction in range of motion and an overall mobility of about 0.6°. The intervertebral mobility of the C3-C4 segment after Zero-P is basically the same as the mean value before surgery, except that the mobility is reduced during bend motion. The overall mobility of the C4-C6 segments are about 1°, and the range of motion is reduced by 92%.

Traditional postoperative surgery has less impact on the stress on the two-segments nucleus pulposus, but there is stress concentration in the end plate. Theoretical values judge that there is a risk of continued wear and degradation after surgery; While the overall stress level of the Zero-P endplate became stable without obvious stress concentration, and the postoperative simulation results were relatively stable.

Based on the stress variation patterns of the traditional anterior approach model and the Zero-P model obtained in this study, spine surgeons can choose surgical techniques more flexibly and develop different surgical plans for patients with different degrees of disease. For example, for patients with multilevel cervical spondylosis, if degeneration is observed in the superior level of the affected segments before surgery, the Zero-P decompression and fusion procedure can be considered. This can avoid the increase in intervertebral disc stress at the superior level of the fusion site caused by the traditional anterior approach with a plate. However, if a patient has significant abnormal cervical curvature or cervical kyphosis before surgery, the traditional anterior approach with plate fixation can be prioritized for better reconstruction of the overall cervical curvature.

The maximum stress of both internal fixation screws is within the allowable range and can meet the needs of use. However, the extreme value of the cyclic stress of the fixing screw of the Zero-P method is nearly doubled, and theoretically its service life will be shorter than that of the traditional method. The connecting plate that matches the C5-C6 segment's nail hole is the typical titanium plate's risk location. After surgery, there is a chance that the titanium plate will slip or fail from fatigue due to the left-rotation. It is recommended to pay attention to the reserved installation distance between the titanium plate and the segments and the fitting of the physiological curvature to avoid the impact of the titanium plate on the vertebrae when the patient undergoes excessive flexion and extension movements after surgery.

The Zero-P cage's entire component has a clearly visible unequal and concentrated stress distribution. The width of the cage and the modification of the vertebral body fixation surface after disc excision during surgery have a direct impact on the postoperative interaction between the vertebrae and the instrument. The stress effect on the cage's edge could be the primary cause of fatigue failure. At the same time, the vertebral body's corresponding contact location is at risk of accelerated wear. It is advised to pay close attention to the stress dispersion design of the cage's edge. This includes, but is not limited to, modifying the edge generatrix and increasing the series of edge interaction parameters for clinical selection based on specific lesion conditions.

REFERENCES

[1] D. Zhou, J. Ding, J. Ya, L. Pan, F. Yan, Q. Yang, Y. Ding, X. Ji, and R. Meng, "Understanding jugular venous outflow disturbance," *CNS Neurosci. Therapeutics*, vol. 24, no. 6, pp. 473–482, Jun. 2018.

[2] W.-S. Lin, T.-F. Huang, T.-Y. Chuang, C.-L. Lin, and C.-H. Kao, "Association between cervical spondylosis and migraine: A nationwide retrospective cohort study," *Int. J. Environ. Res. Public Health*, vol. 15, no. 4, p. 587, Mar. 2018.

[3] S. P. Cohen and W. M. Hooten, "Advances in the diagnosis and management of neck pain," *Brit. Med. J.*, vol. 358, Aug. 2017, Art. no. j3221.

[4] M. Nedelmann, M. Kaps, and W. Mueller-Forell, "Venous obstruction and jugular valve insufficiency in idiopathic intracranial hypertension," *J. Neurol.*, vol. 256, no. 6, pp. 964–969, Jun. 2009.

[5] F. Doepp, J. Valdueza, and S. Schreiber, "Incompetence of internal jugular valve in patients with primary exertional headache: A risk factor?" *Cephalalgia*, vol. 28, no. 2, pp. 182–185, Feb. 2008.

[6] K. Murakami, K. Nagata, H. Hashizume, H. Oka, S. Muraki, Y. Ishimoto, M. Yoshida, S. Tanaka, A. Minamide, Y. Nakagawa, N. Yoshimura, and H. Yamada, "Prevalence of cervical anterior and posterior spondylolisthesis and its association with degenerative cervical myelopathy in a general population," *Sci. Rep.*, vol. 10, no. 1, p. 10455, Jun. 2020.

[7] J. Ding, D. Zhou, L. Pan, J. Ya, C. Liu, F. Yan, C. Fan, Y. Ding, X. Ji, and R. Meng, "Cervical spondylotic internal jugular venous compression syndrome," *CNS Neurosci. Therapeutics*, vol. 26, no. 1, pp. 47–54, Jan. 2020.

[8] L. Zhang and H. Wang, "A novel segmentation method for cervical vertebrae based on PointNet++ and converge segmentation," *Comput. Methods Programs Biomed.*, vol. 200, Mar. 2021, Art. no. 105798.

[9] M. G. Kaiser, R. W. Haid, B. R. Subach, B. Barnes, and G. E. Rodts, "Anterior cervical plating enhances arthrodesis after discectomy and fusion with cortical allograft," *Neurosurgery*, vol. 50, no. 2, pp. 229–238, Feb. 2002.

[10] S. Zheng, G. Liang, J. Chen, Q. Duan, and Y. Chang, "Severity assessment of cervical spondylotic myelopathy based on intelligent video analysis," *IEEE J. Biomed. Health Informat.*, vol. 26, no. 9, pp. 4486–4496, Sep. 2022.

[11] Y. H. Lee, S. Kim, J.-S. Suh, and D. Hwang, "Learning radiologist's step-by-step skill for cervical spinal injury examination: Line drawing, prevertebral soft tissue thickness measurement, and swelling detection," *IEEE Access*, vol. 6, pp. 55492–55500, 2018.

[12] G. Liu, W. Jia, M. Wang, A. A. Heidari, H. Chen, Y. Luo, and C. Li, "Predicting cervical hyperextension injury: A covariance guided sine cosine support vector machine," *IEEE Access*, vol. 8, pp. 46895–46908, 2020.

[13] Á. Bernabéu-Sanz, J. V. Mollá-Torró, S. López-Celada, P. M. López, and E. Fernández-Jover, "MRI evidence of brain atrophy, white matter damage, and functional adaptive changes in patients with cervical spondylosis and prolonged spinal cord compression," *Eur. Radiol.*, vol. 30, no. 1, pp. 357–369, Jan. 2020.

[14] A. L. Asher, C. J. Devin, P. Kerezoudis, S. Chotai, H. Nian, F. E. Harrell, Jr., A. Sivaganesan, M. J. McGirt, K. R. Archer, K. T. Foley, P. V. Mummaneni, E. F. Bisson, J. J. Knightly, C. I. Shaffrey, and M. Bydon, "Comparison of outcomes following anterior vs posterior fusion surgery for patients with degenerative cervical myelopathy: An analysis from quality outcomes database," *Neurosurgery*, vol. 84, no. 4, pp. 919–926, Apr. 2019.

[15] C. M. DuBois, P. M. Bolt, A. G. Todd, P. Gupta, F. T. Wetzel, and F. M. Phillips, "Static versus dynamic plating for multilevel anterior cervical discectomy and fusion," *Spine J.*, vol. 7, no. 2, pp. 188–193, Mar. 2007.

[16] P. Wang, M. Tang, L. Zhou, Z. J. Xu, and K. Yang, "Finite element analysis of fixation stability of cervical vertebra single door with microtitanium plate," *Chin. J. Orthopaedic Surg.*, vol. 29, no. 22, pp. 2072–2077, 2021.

[17] J.-C. Wu, H.-K. Chang, W.-C. Huang, and Y.-C. Chen, "Risk factors of second surgery for adjacent segment disease following anterior cervical discectomy and fusion: A 16-year cohort study," *Int. J. Surg.*, vol. 68, pp. 48–55, Aug. 2019.

[18] C. L. A. Vleggeert-Lankamp, T. M. H. Janssen, E. van Zwet, C. M. W. Goedmakers, L. Bosscher, W. Peul, and M. P. Arts, "The NECK trial: Effectiveness of anterior cervical discectomy with or without interbody fusion and arthroplasty in the treatment of cervical disc herniation; a double-blinded randomized controlled trial," *Spine J.*, vol. 19, no. 6, pp. 965–975, Jun. 2019.

[19] E. M. Soffin, D. S. Wetmore, L. A. Barber, A. S. Vaishnav, J. D. Beckman, T. J. Albert, C. H. Gang, and S. A. Qureshi, "An enhanced recovery after surgery pathway: Association with rapid discharge and minimal complications after anterior cervical spine surgery," *Neurosurgical Focus*, vol. 46, no. 4, p. E9, Apr. 2019.

[20] C. S. Carrier, C. M. Bono, and D. R. Lebl, "Evidence-based analysis of adjacent segment degeneration and disease after ACDF: A systematic review," *Spine J.*, vol. 13, no. 10, pp. 1370–1378, Oct. 2013.

[21] B. Debono, M. V. Corniola, R. Pietton, P. Sabatier, O. Hamel, and E. Tessitore, "Benefits of enhanced recovery after surgery for fusion in degenerative spine surgery: Impact on outcome, length of stay, and patient satisfaction," *Neurosurgical Focus*, vol. 46, no. 4, p. E6, Apr. 2019.

[22] J. C. Wu, G. F. Fang, G. H. Lai, W. D. Zhuang, X. W. Li, H, Wang, and H. X. Sang, "Clinical efficacy of Hybrid anterior cervical surgery in the treatment of double or multi-level cervical spondylosis," *Chin. Clin. New Med.*, vol. 16, no. 3, pp. 207–212, 2023.

[23] X. Zhao, and W. Yuan, "Biomechanical analysis of cervical range of motion and facet contact force after a novel artificial cervical disc replacement," *Amer. J. Transl. Res.*, vol. 11, no. 5, pp. 3109–3115, 2019.

[24] R. B. Delamarter and J. Zigler, "Five-year reoperation rates, cervical total disc replacement versus fusion, results of a prospective randomized clinical trial," *Spine*, vol. 38, no. 9, pp. 711–717, Apr. 2013.

[25] P. K. Pandey, I. Pawar, J. Gupta, and R. R. Verma, "Comparison of outcomes of single-level anterior cervical discectomy with fusion and single-level artificial cervical disc replacement for single-level cervical degenerative disc disease," *Spine*, vol. 42, no. 1, pp. E41–E49, Jan. 2017.

[26] Y. Chen, H. Chen, P. Cao, and W. Yuan, "Anterior cervical interbody fusion with the zero-P spacer: Mid-term results of two-level fusion," *Eur. Spine J.*, vol. 24, no. 8, pp. 1666–1672, Aug. 2015.

[27] Y. Chen, Y. Liu, H. Chen, P. Cao, and W. Yuan, "Comparison of curvature between the zero-P spacer and traditional cage and plate after 3-level anterior cervical discectomy and fusion: Mid-term results," *Clin. Spine Surg., Spine Publication*, vol. 30, no. 8, pp. E1111–E1116, Oct. 2017.

[28] Q. Wang, S. Y. Li, Y. Xiong, and T. T. Li, "Biomechanical changes of cervical vertebrae in internal fixation with different anterior cervical interbody fusion systems," *Res. Tissue Eng. China*, vol. 28, no. 6, pp. 821–826, 2023.

[29] X.-F. Li, L.-Y. Jin, C.-G. Liang, H.-L. Yin, and X.-X. Song, "Adjacent-level biomechanics after single-level anterior cervical interbody fusion with anchored zero-profile spacer versus cage-plate construct: A finite element study," *BMC Surg.*, vol. 20, no. 1, p. 66, Apr. 2020.

[30] T.-K. Wu, Y. Meng, H. Liu, B.-Y. Wang, Y. Hong, X. Rong, C. Ding, and H. Chen, "Biomechanical effects on the intermediate segment of noncontiguous hybrid surgery with cervical disc arthroplasty and anterior cervical discectomy and fusion: A finite element analysis," *Spine J.*, vol. 19, no. 7, pp. 1254–1263, Jul. 2019.

[31] R.-C. Dong, Q.-J. Guo, W. Yuan, W. Du, X.-H. Yang, and Y.-J. Zhao, "The finite element model of seated whole human body for vibration investigations of lumbar spine in complex system," *IEEE Access*, vol. 8, pp. 125046–125055, 2020.

[32] X. Sun, H. Wang, W. Wang, N. Li, T. Hämäläinen, T. Ristaniemi, and C. Liu, "A statistical model of spine shape and material for population-oriented biomechanical simulation," *IEEE Access*, vol. 9, pp. 155805–155814, 2021.

[33] B. Q. Li,Z. Yu, Z. H. Xu, and L. L. Dong, "Finite element analysis of biomechanical effects of anterior cervical single level decompression fusion and decompression fusion combined with plate internal fixation on adjacent segments," *China Med. Eng.*, vol. 30, no. 10, pp. 5–17, 2022.

[34] N. Nishida, S. Tripathi, M. Mumtaz, A. Kelkar, Y. Kumaran, T. Sakai, and V. K. Goel, "The effect of anterior-only, posterior-only, and combined anterior posterior fixation for cervical spine injury with soft tissue injury: A finite element analysis," *World Neurosurgery*, vol. 171, pp. e777–e786, Mar. 2023.

[35] X. Zhang, Y. Yang, Y.-W. Shen, K.-R. Zhang, L.-T. Ma, C. Ding, B.-Y. Wang, Y. Meng, and H. Liu, "Biomechanical performance of the novel assembled uncovertebral joint fusion cage in single-level anterior cervical discectomy and fusion: A finite element analysis," *Frontiers Bioeng. Biotechnol.*, vol. 11, Mar. 2023, Art. no. 931202.

[36] T. Zhang, N. Guo, G. Gao, H. Liu, Y. Li, F. Gao, Q. Zhang, X. Tao, W. Yang, and Y. Wang, "Comparison of outcomes between Zero-p implant and anterior cervical plate interbody fusion systems for anterior cervical decompression and fusion: A systematic review and meta-analysis of randomized controlled trials," *J. Orthopaedic Surg. Res.*, vol. 17, no. 1, p. 47, Jan. 2022.

[37] P. Ye, R. Fu, and Z. Wang, "Topological optimization of anterior cervical plate (ACP) and its biomechanic characteristics," *Bio-Med. Mater. Eng.*, vol. 34, no. 6, pp. 525–535, Nov. 2023.

[38] S. P. Moroney, A. B. Schultz, J. A. A. Miller, and G. B. J. Andersson, "Load-displacement properties of lower cervical spine motion segments," *J. Biomechanics*, vol. 21, no. 9, pp. 769–779, Jan. 1988.
[39] M. Panjabi, R. Brand, and A. White, "Mechanical properties of the human thoracic spine as shown by three-dimensional load-displacement curves," *J. Bone Joint Surg.*, vol. 58, no. 5, pp. 642–652, Jul. 1976.

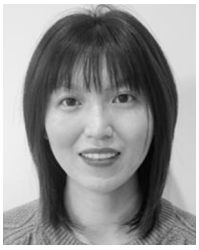

DAN LI was born in Tangshan, Hebei, China, in 1988. She received the B.S. and M.S. degrees in mechanical engineering from Dalian Jiaotong University, China, in 2015.

She is the author of three books, more than 12 articles, and more than three inventions. Her research interests include biomechanics, finite element methods, and medical device design.

Ms. Li was a core member of Hunan Province Education Science Project, in 2020, and the National Resource Library Construction Project, in 2022.

YUTING YU received the B.Sc. degree in biomedical engineering from Shandong University of Science and Technology, China, and the M.S. degree from Lanzhou Jiaotong University. She is currently pursuing the Ph.D. degree with Universiti Teknologi MARA, Malaysia. After completing the bachelor's degree, she works with the Equipment Department, Juye Coal Field Central Hospital. Her main research interests include biomedical image research and bioelectronics.

DONG CHAO was born in Taiyuan, Shanxi, China, in 1989. He received the B.S. and M.S. degrees in mechanical engineering from Dalian Jiaotong University, China, in 2015.

He is the author of more than six articles and more than five inventions. His research interests include biomechanics, finite element methods, and mechanical design theory.

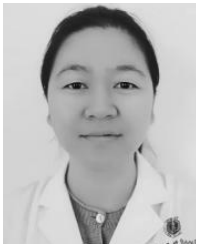

QINGQING YU received the B.Eng. degree in biomedical engineering from Shandong University of Science and Technology. She is currently an Engineer with the Equipment Department, PKU Care Luzhong Hospital. She is primarily responsible for maintenance, quality control, and calibration of medical equipment. As an Expert with the Pharmaceutical Vigilance Team, Zibo, Shandong, she has actively participated in the national key monitoring of adverse events related to medical devices during the 14th Five-Year Plan in China.